Contents lists available at SCCE

Journal of Soft Computing in Civil Engineering

Journal homepage: www.jsoftcivil.com

Adaptive Neuro-Fuzzy and Simple Adaptive Control Methods for Attenuating the Seismic Responses of Coupled Buildings with Semi-Active Devices: Comparative Study

O.A.S. Al-Fahdawi[1*], L.R. Barroso[2], R.W. Soares[1]

1. Ph.D. Candidate, Texas A&M University, Zachry Department of Civil and Environmental Engineering, College Station, TX 77843, United States
2. Associate Professor, Texas A&M University, Zachry Department of Civil and Environmental Engineering, College Station, TX 77843, United States
Corresponding author: *omarahmed1984@tamu.edu*

https://doi.org/10.22115/SCCE.2019.199731.1128

ARTICLE INFO

Article history:
Received: 15 September 2019
Revised: 12 October 2019
Accepted: 16 October 2019

Keywords:
Coupled buildings;
Adaptive control;
Adaptive neuro-fuzzy;
SAC method;
MR damper.

ABSTRACT

This paper describes two adaptive control methods for mitigating the seismic responses of two connected buildings with MR dampers at different levels. First method developed in this study is the adaptive neuro-fuzzy controller which consists of a fuzzy logic controller provided with learning algorithm based on adaptive neural networks. The learning algorithm is implemented to modify the parameters of the fuzzy logic controller such that its outputs track the behavior of predetermined training data. Second method is the simple adaptive controller which falls into the category of model-following adaptive strategies. In this method, a plant is commanded to follow a well-designed reference-model with desirable trajectories through a closed loop action. The coupled system consists of two adjacent buildings having different heights in order to separate the model shapes of the individual buildings. Different types of feedbacks such as displacement, velocity, and acceleration are employed to identify their impacts on the performance of the developed adaptive controllers. Numerical analyses are carried out for the complex system assuming no change in the nominal design parameters and then for the system where a change in these parameters is introduced. The results reveal that using the adaptive controllers developed in this study to regulate the MR dampers connecting the two adjacent buildings can successfully alleviate the seismic responses under various types and intensities of earthquakes.

How to cite this article: Al-Fahdawi OAS, Barroso LR, Soares RW. Adaptive neuro-fuzzy and simple adaptive control methods for attenuating the seismic responses of coupled buildings with semi-active devices: comparative study. J Soft Comput Civ Eng 2019;3(3):01–21. https://doi.org/10.22115/scce.2019.199731.1128.

1. Introduction

Protection of civil structures from undesirable vibrations due to natural hazards is crucial for sustaining structural integrity. One of the creative ideas to withstand these events is inter-connecting closely spaced buildings with single or multiple links. Coupling of such structures has recognized to be architecturally and functionally beneficial. Structural performance of coupled structures can be improved by implementing control devices within these links to dissipate energy, an approach that has been verified effective for reducing the structural responses.

Control studies are usually divided in civil engineering applications into two categories: one focuses on safety and the other its main concern is functionality. The goal of the former type is to use the energy dissipative devices to decrease major displacement and inter-story drifting. However, when functionality is the most important as in the design of tall and slender buildings, control is utilized to attenuate the structural acceleration in order to increase occupant comfort during relatively mild events [1].

Improving the structural performance of coupled buildings has been reported in the use of passive links [2,3]. More advanced strategies were implemented by using active control devices to connect high-rise buildings such as hydraulic actuators [4–6]. In addition to the analytical studies, there are few experimental studies on the coupled buildings [6,7]. A high-power demand and instability potential associated with active devices have made semi-active devices been embraced by researchers because of their potential in remedying these issues and showing effective performance abilities which make them ideal for civil engineering applications [8,9]. One of the most sophisticated control devices is the magneto-rheological (MR) damper which exhibits a great potential for use in vibration control. The MR damper has been utilized in many studies to connect adjacent buildings to attenuate seismic responses [10–14]. The device needs a small amount of power to operate and it can continue to work as a passive device in case of failure of the power supply or the control algorithm. The yield strength of the MR fluid can be changed by controlling the electrical current in the coil [15]. The simple Bouc-Wen model is utilized to model the hysteretic behavior of the MR damper. This model combines linear dashpot element and the Bouc-Wen element which describes the hysteretic behavior of the MR damper. The performance of the simple Bouc-Wen model was investigated by Wong et al. [16] and compared to experimental data. The results showed that the proposed model perfectly matched the experimental data except near small velocities. Spencer et al. [17] remedied this shortcoming by imposing additional parameters to the classical Bouc-Wen model. The MR damper has been successfully implemented in different civil structures such as the Nihon-Kagaku-Miraikan, the Tokyo National Museum of Emerging Science and Innovation (300 kN capacity) in Japan, Dongting Lake Bridge in Hunan, China, the Binzhou Yellow River Bridge in China, residential buildings (400 kN capacity) in Japan.

Despite the remarkable accomplishments of classical control design, its performance seems to be restricted since it cannot cope with uncertainties and time-varying parameters in real world applications [18]. Adaptive control is more suitable for uncertain systems with time-varying

parameters because it applies the right control command to the right situation as the control command is modified online in order to cope with such systems [19].

In this paper, the adaptive neuro-fuzzy inference systems (ANFIS) and the simple adaptive controller (SAC) are used. ANFIS, which is categorized as an intelligent control, is based on Sugeno fuzzy model which integrates both the fuzzy logic controller (FLC) with adaptive neural networks in one framework. This method has set of rules corresponding to fuzzy IF-THEN statements, but with learning capabilities to simplify nonlinear relations into simplistic verbose statements. In particular, the fuzzy logic controller has been used in many research to regulate semi-active devices [20,21]. The learning capability of ANFIS comes from the artificial neural networks which try to emulate the biological neurons of the human brain [22]. SAC, however, is one of the model following schemes in which an uncertain system is required to track the behavior of a reference model with pre-defined trajectories[23,24]. SAC was implemented in different fields. For example, in aerospace engineering, SAC was used by Ulrich et al. [25] to overcome the problem of the adaptive feedback in the spacecrafts under unknown parametric uncertainties. Few studies have used SAC in civil engineering field to deal with parameters changing under hazardous events [26,27].

The purpose of this paper is to investigate the efficiency of two adaptive control methods, ANFIS and SAC, in attenuating the seismic responses of two connected buildings with MR dampers. Different feedback types for both ANFIS and SAC are tested to identify the impact of each feedback type on the performance of each method. The following feedback schemes are investigated in this paper:

1.1. Displacement feedback for both ANFIS and SAC which is labeled as “ANFIS1” and “SAC1”, respectively.

1.2. Velocity feedback for both ANFIS and SAC which is labeled as “ANFIS2” and “SAC2”, respectively.

1.3. Acceleration feedback for both ANFIS and SAC which is labeled as “ANFIS3” and “SAC3”, respectively.

1.4. Combined velocity and acceleration feedbacks for ANFIS only which is labeled as “ANFIS4”.

2. Modeling of the coupled system

The coupled system is modeled as two shear type buildings with different heights. The mass of each floor is assumed to be lumped at its center and the corresponding floors are assumed to be colinear. Number of unconnected floors is n_1 and number of connected floors is n_2. Therefore, the total number of floors in the coupled system is $n_1 + 2n_2$, as shown in Fig. 1 [28]. The system is assumed to be subjected to same uni-directional earthquake excitation neglecting its waveform, and soil-structure interaction effect is also neglected.

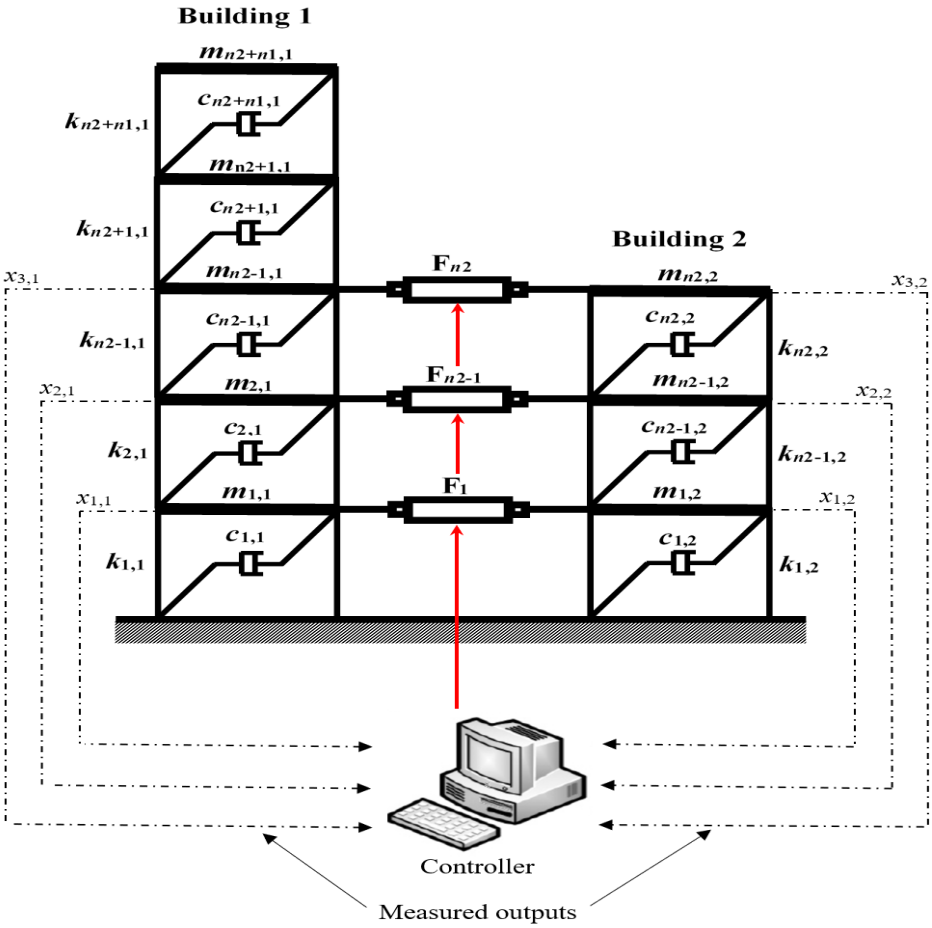

Fig. 1. The structural system along with the control system layout [28].

The equation of motion of the coupled system under seismic excitation can be written in a compact form as:

$$[M_s]\{\ddot{x}(t)\}+[C_s]\{\dot{x}(t)\}+[K_s]\{x(t)\}=[J]\{f_m(t)\}-[M_s]\{\Lambda\}\{\ddot{x}_g(t)\} \tag{1}$$

where M_s, C_s, and K_s are the mass, damping and stiffness matrices of the coupled system, respectively. $f_m(t)$ is the vector of the control forces; J is the distribution matrix of the control devices; $x(t)$, $\dot{x}(t)$, and $\ddot{x}(t)$ are the relative displacement, velocity, and acceleration vectors, respectively. $\{\Lambda\}$ is a vector with all ones; $\ddot{x}_g(t)$ is the ground acceleration vector.

The structural mass, stiffness, and damping matrices of the structural system are written as follows:

$$M_{s(n_1+2n_2,n_1+2n_2)}=\begin{bmatrix}[M_1]_{(n_1+n_2,n_1+n_2)} & [0]_{(n_1+n_2,n_2)}\\ [0]_{(n_2,n_1+n_2)} & [M_2]_{(n_1+n_2,n_1+n_2)}\end{bmatrix} \tag{2}$$

$$K_{s(n_1+2n_2,n_1+2n_2)}=\begin{bmatrix}[K_1]_{(n_1+n_2,n_1+n_2)} & [0]_{(n_1+n_2,n_2)}\\ [0]_{(n_2,n_1+n_2)} & [K_2]_{(n_1+n_2,n_1+n_2)}\end{bmatrix}+[K_c] \tag{3}$$

$$C_{s(n_1+2n_2,n_1+2n_2)}=\begin{bmatrix}[C_1]_{(n_1+n_2,n_1+n_2)} & [0]_{(n_1+n_2,n_2)}\\ [0]_{(n_2,n_1+n_2)} & [C_2]_{(n_1+n_2,n_1+n_2)}\end{bmatrix}+[C_c] \tag{4}$$

where M_1 and M_2, K_1 and K_2, and C_1 and C_2 are mass, stiffness, and damping matrices of Building 1 and 2, respectively. K_c and C_c are mapping matrices developed to transfer the link's stiffness and damping properties to the stiffness and damping matrices of the peripheral structures and they are defined as:

$$K_{c(n_1+2n_2,n_1+2n_2)}=\begin{bmatrix}[K_d]_{(n_2,n_2)} & [0]_{(n_2,n_1)} & -[K_d]_{(n_2,n_2)}\\ [0]_{(n_1,n_2)} & [0]_{(n_1,n_1)} & [0]_{(n_1,n_2)}\\ -[K_d]_{(n_2,n_2)} & [0]_{(n_2,n_1)} & [K_d]_{(n_2,n_2)}\end{bmatrix} \tag{5}$$

$$C_{c(n_1+2n_2,n_1+2n_2)}=\begin{bmatrix}[C_d]_{(n_2,n_2)} & [0]_{(n_2,n_1)} & -[C_d]_{(n_2,n_2)}\\ [0]_{(n_1,n_2)} & [0]_{(n_1,n_1)} & [0]_{(n_1,n_2)}\\ -[C_d]_{(n_2,n_2)} & [0]_{(n_2,n_1)} & [C_d]_{(n_2,n_2)}\end{bmatrix} \tag{6}$$

where the K_d and C_d are matrices with stiffness and damping coefficients of the links. The dynamic characteristics of the connectors are assumed to stay unchanged during earthquakes. The distribution matrix of the control forces, J, is defined as follows:

$$J_{(n_1+2n_2,n_1+2n_2)}=\begin{bmatrix}[I]_{(n_2,n_1+2n_2)}; & [0]_{(n_1,n_2+2n_2)}\\ [0]_{(n_2,n_1+n_2)}, & -[I]_{(n_2,n_2)}\end{bmatrix} \tag{7}$$

where $[I]$ is the identity matrix. The negative sign in equation (7) refers to that the control forces are acting in opposite directions on both buildings.

3. Adaptive control

Adaptive control strategy has a capability to adjust its own parameters automatically based on an operative situation. The advantage of implementing adaptive control is to enhance the structural performance in the presence of uncertainties and parametric changes. This paper introduces two adaptive control methods that are developed to regulate the MR dampers that connect two closely-spaced buildings.

3.1. Adaptive neuro-fuzzy inference system

The effectiveness of the fuzzy logic controller is dependent on verbose rules that are needed to define the correlation between the inputs and outputs. These rules in most of the times are determined based on expert knowledge. Adaptive Neuro-Fuzzy Inference system (ANFIS) is utilized to facilitate the adaptation and learning ability of the adaptive system in a way that makes the system less dependent on expert knowledge. The architecture of ANFIS consists of a number of fuzzy IF-THEN statements that are written based on Sugeno model as follows [29,30]:

Rule 1. If x is A_1 and y is B_1 then $f_1 = p_1 x + q_1 y + r_1$

Rule 2. If x is A_2 and y is B_2 then $f_2 = p_2 x + q_2 y + r_2$

Rule n. If x is A_n and y is B_n then $f_n = p_n x + q_n y + r_n$

where x and y are the inputs and $A_1 \ldots A_n$ and $B_1 \ldots B_n$ are fuzzy membership functions. $f_1 \ldots f_n$ are the fuzzy outputs based upon the fuzzy rules. p_i, q_i, and r_i are parameters that are defined during the training process. The inputs x and y are "antecedent" variables and f_i is a "consequent" variable of the rule i. The rules above are implemented in ANFIS as in Fig. 2 in which the squares represent adaptive nodes and circles represent stationary (fixed) nodes. ANFIS utilizes a hybrid-learning technique to establish an input–output mapping based on the input–output data pairs collected from simulation. The hybrid strategy uses a combination of "steepest-descent" method and least-squares estimation technique to adjust the fuzzy membership functions.

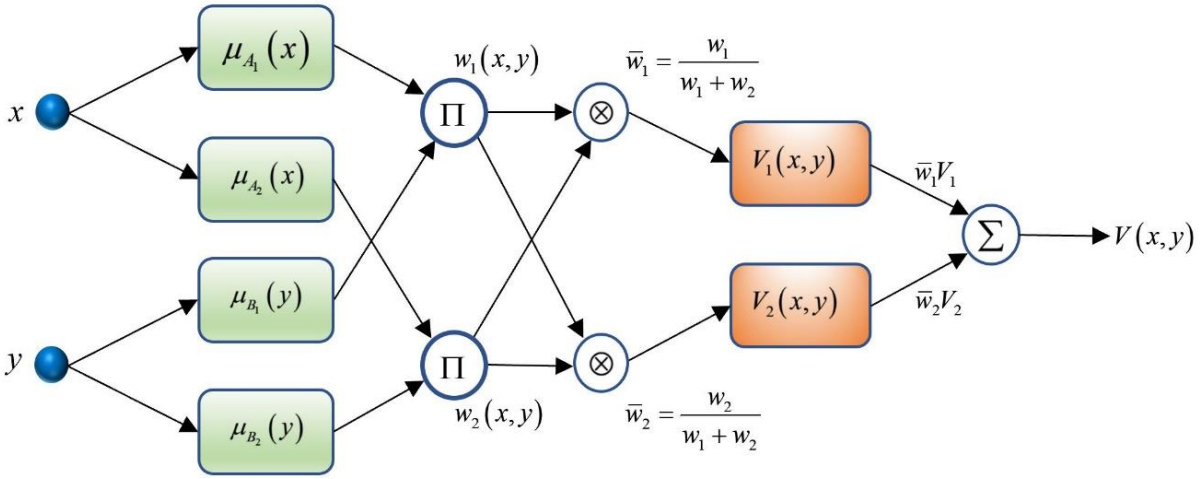

Fig. 2. ANFIS architecture.

In the first layer of Fig. 2 represented by squared nodes, ANFIS maps the inputs (crisp) to the fuzzy membership functions and the outputs of this layer is determined as follows:

$$Q_i^1 = \mu_{A_i}(x_i),\ i = 1,2,$$
$$Q_i^1 = \mu_{B_{i-2}}(y_i),\ i = 3,4, \tag{8}$$

where μ is a weight obtained from the fuzzy membership function. In the second layer, simple multiplication of the outputs of layer 1 as follows:

$$Q_i^2 = w_i = \mu_{A_i}(x_i)\,\mu_{B_i}(y_i),\ i = 1,2, \tag{9}$$

A normalization of the outputs of the second layer is conducted in the third layer. The outputs of this layer is represented as follows:

$$Q_i^3 = \overline{w}_i = \frac{w_i}{w_1 + w_2},\ i = 1,2, \tag{10}$$

The fourth layer represents the product of the outputs of the third layer and a first-order Sugeno model. The outputs of this layer can be given by:

$$Q_i^4 = \overline{w}_i V_i = \overline{w}_i\left(p_i x + q_i y + r_i\right),\ i = 1,2, \tag{11}$$

The fifth layer is only one fixed node that performs the summation of all coming signals. Hence, the output of this layer represents the overall output of the model as follows:

$$Q_i^5 = \sum_{i=1}^{2} \overline{w}_i V_i = \frac{\sum_{i=1}^{2} w_i V_i}{w_1 + w_2} \tag{12}$$

The adaptive neural network (learning algorithm) task is to tune all the fuzzy logic controller's parameters (p_i, q_i, and r_i) until the error between the fuzzy model and the input (e.g. acceleration) – output (voltage) data pairs (training data) is sufficiently small or attain a pre-defined epoch.

The training data are produced by using Linear Quadradic Regulator (LQR) designed for this purpose assuming full-state feedback. The training data should be representative of different situations under different excitations during the operation of the controller [8]. Also, there must be enough training data available for the fuzzy controller; otherwise, the mount of interpolation by the fuzzy controller would be excessive [31]. An external disturbance is used to define the range and type of actual excitations which the fuzzy controller is employed to handle. The disturbance used by the target controller is created through band-limited Gaussian white noise built in SIMULINK with a duration of 80 s. The parameters of the LQR are chosen as follows:

$$Q_{(2n_1+2n_2,\,2n_1+2n_2)} = \frac{1}{2}\begin{bmatrix} [K_s]_{(n_1+2n_2,\,n_1+2n_2)} & [0]_{(n_1+2n_2,\,n_1+2n_2)} \\ [0]_{(n_1+2n_2,\,n_1+2n_2)} & [M_s]_{(n_1+2n_2,\,n_1+2n_2)} \end{bmatrix} \tag{13}$$

$$R_{(2n_1,2n_1)} = \rho I_{(2n_1,2n_1)};\ \rho = 1\times10^{-5}$$

where K_s and M_s are the stiffness and mass matrices of the coupled system. The primary fuzzy logic controller developed in the current paper employs one and two inputs, respectively to infer the command voltage. Seven Gaussian membership functions are defined the input data, as shown in Fig. 3. The fuzzy sets for the input variables are PL = positive large, PM = positive

medium, PS = positive small, ZE = zero, NL = negative large, NM = negative medium, NS = negative small. The fuzzy sets for the output (voltage) variable are ZE = zero, M = medium, and L = large. The maximum applied voltage for the MR damper is saturated to 10 V. Since different inputs considered in this study, range of the universe of discourse will vary based on the input type. For instance, if the input variable is the displacement, the range is defined from -1 to 1. On the other hand, if the input is the acceleration, the range is chosen to be from -15 to 15. If the range of the universe of discourse does not accommodate all values of the input variable, the software will return error message.

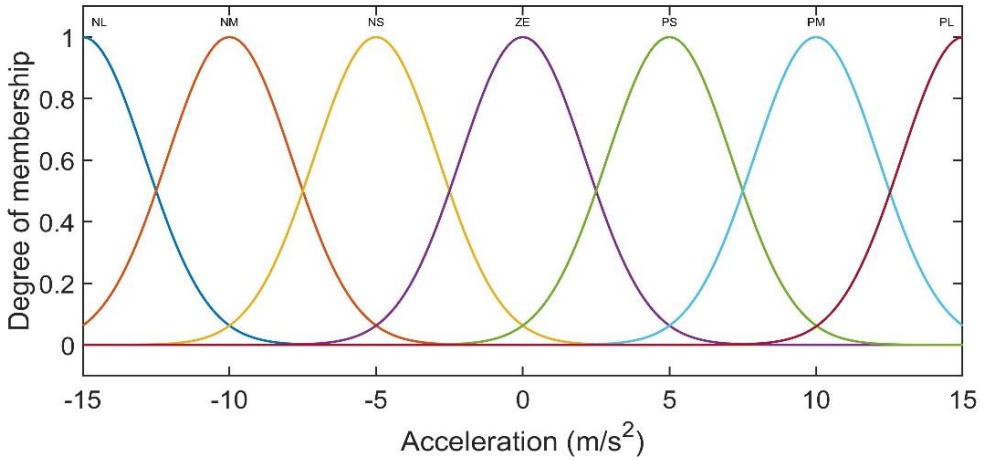

Fig. 3. Primary input membership functions for the FLC.

3.2. SAC algorithm

According to SAC, the behavior of the actual structural system (plant) is characterized by pre-defined outputs of a reference-model. To achieve a quality tracking between the plant and the reference-model, SAC modifies the control output by monitoring the tracking error between both systems. Fig. 4 shows the block diagram of SAC scheme. The state-space representation of the equation of motion of the coupled system derived in equation (1) can be written as follows:

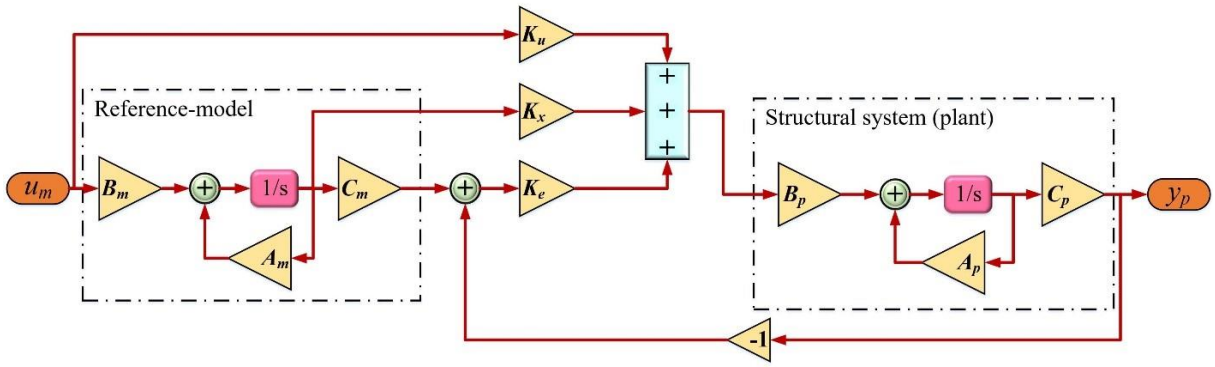

Fig. 4. Block diagram of SAC.

$$\dot{x}_p(t) = A_p x_p(t) + B_p u_p(t) + d_i(t)$$
$$y_p(t) = C_p x_p(t) + D_p u_p(t) + d_o(t) \quad (14)$$

where A_p and B_p are the system and input matrices, respectively. C_p is the plant output matrix, x_p is the state vector, y_p is the plant output vector, u_p is the control input vector, and d_i and d_o are bounded input and output plant disturbances, respectively. The output of the system characterized in equation (14) is required to follow the output of the following reference-model:

$$\begin{aligned} \dot{x}_m(t) &= A_m x_m(t) + B_m u_m(t) \\ y_m(t) &= C_m x_m(t) + D_m u_m(t) \end{aligned} \tag{15}$$

The reference-model above is selected to produce the desired output for the actual system to follow, yet the reference-model does not have to be the result of a prior modeling of the plant [32].

The adaptive control command, $u_p(t)$, persistently attempts to bring the error, $e_y(t) = y_m(t) - y_p(t)$, to zero. $u_p(t)$ is determined as follows:

$$u_p(t) = K(t) r(t) \tag{16}$$

where $r(t)$ is the reference vector and $K(t)$ is the adaptive gain matrix. $r(t)$ and $K(t)$ are defined as follows:

$$r^T(t) = \left[\left(y_m(t) - y_p(t) \right)^T \quad x_m^T(t) \quad u_m^T(t) \right] \tag{17}$$

$$K(t) = K_I(t) + K_p(t) \tag{18}$$

where $K_p(t)$ and $K_I(t)$ are the proportional and the integral adaptive gains, and they are written as follows:

$$\dot{K}_I(t) = e_y(t) r(t)^T T - \sigma K_I(t) \tag{19}$$

$$K_p(t) = e_y(t) r(t)^T \bar{T} \tag{20}$$

where T and $\bar{T}$ are tuning matrices need to be tuned by the control designer to regulate the adaptation rate. The integral gain, $K_I(t)$, is required for the adaptation stability and speeding up the convergence, while the proportional gain, $K_p(t)$, is utilized because it can improve the plant performance and facilitate the perfect tracking by adding immediate forfeit on large errors. In equation (19), the σ-term is used to save the integral gain from divergence in the presence of disturbances and it can be very small number [33].

The reference-model should behave better than the actual system in order to enhance its structural performance. For this purpose, an ideal LQR with parameters shown in equation (13) is utilized to determine the desired behavior of the reference-model. In real-world applications, it is difficult to achieve perfect tracking because of the control system's limitations.

4. Modeling of the MR damper

Modeling of the MR damper is crucial in predicting the behavior of the controlled system. The simple Bouc-Wen model, depicted in Fig. 5, has been proved to precisely track the hysteretic behavior of the MR damper over several inputs [34]. The equations governing the behavior of the device are defined as follows [28]:

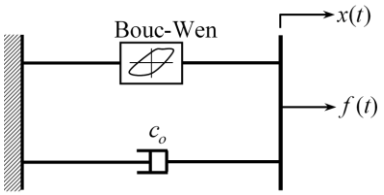

Fig. 5. Schematic of the simple Bouc-Wen model.

$$f(t) = c_o\left[\dot{x}_{B1}(t) - \dot{x}_{B2}(t)\right] + \alpha_o z(t) \tag{21}$$

$$\dot{z}(t) = -\gamma\left|\left[\dot{x}_{B1}(t) - \dot{x}_{B2}(t)\right]\right| z(t)\left|z(t)\right|^{n-1} - \beta\left[\dot{x}_{B1}(t) - \dot{x}_{B2}(t)\right]\left|z(t)\right|^{n} + A\left[\dot{x}_{B1}(t) - \dot{x}_{B2}(t)\right] \tag{22}$$

where $f(t)$ is the generated control force and $z(t)$ is the evolutionary variable that accounts for the hysteretic behavior of the MR damper. $\dot{x}_{B1}$ and $\dot{x}_{B2}$ are the velocity vectors of the connected floors in Building 1 and 2, respectively. c_o and α_o depend on the voltage provided to the device as follows:

$$c_o = c_a + c_b u(t) \tag{23}$$

$$\alpha_o = \alpha_a + \alpha_b u(t) \tag{24}$$

where $u(t)$ is the output of the following filter:

$$\dot{u}(t) = -\eta\left[u(t) - \mathrm{v}\right] \tag{25}$$

Equation (25) is developed to account for the dynamics of the MR damper involved in reaching the rheological equilibrium of the MR fluid [17].

SAC produces control forces required to achieve perfectly tracking between the plant the reference-model. Thus, SAC's output should be converted to power before supplying it to the MR damper. In this study, an inverse model of the MR damper is used to determine the voltage, $V(t)$, required to meet the force generated by SAC. According to the inverse model, the hysteretic variable, $z(t)$, is calculated by equation (26) and then the input to the MR damper and the voltage are determined by equation (27) and equation (28), respectively [35,36]:

$$z(t) \approx \mathrm{sgn}\left(\dot{x}(t)\right)\left(\frac{A}{\gamma + \beta}\right)^{\frac{1}{n}} \tag{26}$$

$$u(t) \approx \frac{f(t) - c_a\dot{x}(t) - \alpha_a z(t)}{c_b\dot{x}(t) + \alpha_b z(t)} \tag{27}$$

$$V(t)=u(t)+\frac{\dot{u}(t)}{\eta} \tag{28}$$

For a 1000 kN capacity MR damper, the following parameters are determined based on optimization and experimental studies Table 1.

Table 1
Parameters of 1000 kN capacity MR damper.

Parameter	Value	Parameter	Value
c_a	4.4×10^2 N.s/m	β	300 m^{-1}
c_b	4.4×10^4 N.s/m	A	1.2
α_a	1.0872×10^7 N/m	n	1.0
α_b	4.9615×10^5 N/mV	η	50 m^{-1}
γ	300 m^{-1}	V_{max}	10 V

5. Comparative study

For the numerical simulations, two buildings (Building 1 and Building 2) with different heights connected at multiple levels are considered. Building 1 has five stories and Building 2 consists of three stories. Number of unconnected floors is n1 and number of connected floors is n2. Therefore, the total number of floors in the coupled system is n_1+2n_2. The mass and stiffness of each floor of both buildings are 4.78×10^5 kg and 1.6983×10^8 N/m, respectively. The total mass and stiffness of Building 1 are 23.9×10^5 kg and 8.4915×10^8 N/m, respectively and the total stiffness of Building 2 is 5.0949×10^8 N/m. The fundamental natural periods of Building 1 and 2 as 1.171 s and 0.749 s, respectively. Thus, the mode shapes of the individual buildings are separated as it is required to make the coupling strategy feasible. Rayleigh formula with 2% damping ratio is used to determine the damping matrix of the combined system. In the current numerical study, the connected floors are the first, second, and third floor.

6. Simulations and analyses

The performance of the proposed structural system is examined when it is subjected to five different seismic events listed in Table 2. Time history analyses of the complex system were conducted in MALAB/SIMULINK R2018a environment. The Dormand-Prince (ode45) solver with variable time step size is used as a primary solver. This method is one of the Runge-Kutta family of ordinary differential equation solvers which uses six function evaluations per step to calculate higher order precise solutions.

Table 2
Selected earthquakes' characteristics.

Earthquake	% Exceedance	PGA (g)	PGV (m/s)	Duration (s)
Landers 1992 (LA10)	10	0.360	0.603	80.00
Northridge 1994 (LA16)	10	0.360	1.007	14.95
Loma Preita 1989 (LA23)	2	0.418	0.737	25.00
Artificial (LS19F)	10	0.784	0.974	81.92
Tabas 1978 (NF01)	Near-field	0.899	1.100	50.00

For the adaptive neuro-fuzzy control method, the number of the input membership functions of the primary fuzzy logic controller is chosen to be seven in Gaussian shape while only three membership functions in bell shape are chosen to represent the output voltage, as shown earlier in Fig. 3 above. These membership functions along with their parameters will be adjusted by the adaptive neural networks based on a situation to match the training data. For SAC method, the tuning values of σ, T and $\bar{T}$ are chosen to be 0.1, $10^3 \times [I]_{31\times31}$ and $10^{10} \times [I]_{31\times31}$ respectively.

The performance of both adaptive control methods is evaluated based on the peak values as well as the overall responses. The peak values of the floor displacement, absolute acceleration, inter-story drift, and base shear are monitored. To assess the peak responses, four evaluation metrics are utilized, as listed in equation (29).

$$J_1 = \frac{\max\left|x_i(t)\right|}{x^{\max}} \qquad J_2 = \frac{\max\left|\ddot{x}_i(t)\right|}{\ddot{x}^{\max}}$$
$$J_3 = \frac{\max\left\{\left|d_i(t)/h_i\right|\right\}}{\delta^{\max}} \qquad J_4 = \frac{\max\left\{\sum_i^n k_i x_i(t)\right\}}{F_b^{\max}} \tag{29}$$

where J_1, J_2, J_3, and J_4 address the peak displacement, absolute acceleration, inter-story drift, and base shear, respectively. The subscript i is the story level and hi is the height of the associated floor. $x^{\max}$and $\ddot{x}^{\max}$ are the maximum displacement and absolute acceleration of the uncontrolled system, respectively. $\delta^{\max}$ and $F_b^{\max}$ are the peak values of the inter-story drift and base shear of the uncontrolled system, respectively. It is obvious that when these criteria are less than unity meaning a reduction in the peak responses has occurred, otherwise, when they are greater than unity, there is an amplification in the peak responses compared to the uncontrolled ones. To evaluate the overall responses of the system, the root-mean-square (RMS) of the structural responses of both buildings is calculated. RMS of a vector is calculated according to the following formula [37]:

$$\left\| . \right\| = \left(\frac{1}{t_f} \int_0^{t_f} [\ . \ ]^2 \, dt \right)^{1/2} \tag{30}$$

The goal of using SAC is to minimize the error between the system's response, $y_p(t)$, and the reference-model's, $y_m(t)$, as possible even with the presence of parameters changing. Similarly, the adaptive neural networks in the ANFIS strategy attempts to monitor the error between the system's responses and the training data and then adjust the parameters of the fuzzy logic controller to decrease the error accordingly. However, the system's outputs would never perfectly match the reference-model's (or training data) trajectories because the control system has limitations such as the ultimate capacity of the control devices.

7. Results and discussion

The time history analyses are conducted on the coupled system considering two cases. First case assumes that the system preserves its dynamic characteristics during the earthquakes which sometimes termed in this study as "undamaged" structure. Second case assumes that the structure experiences some parametric changes during the earthquakes which is sometimes labeled as "damaged" structure. The change in the parameters could be as a result of damage due seismic events, fatigue, temperature fluctuations, … etc. The "damaged" case is reflected in the analysis by reducing the mass by 5% and stiffness by 20%.

Fig. 6 and Fig. 7 display the time histories of Building 1's top floor displacement and acceleration of the undamaged structure with SAC3, ANFIS3, and ANFIS4, respectively subjected to the far-field, LA10, and near-field, NF01, earthquakes, respectively. The results of the undamaged uncontrolled system are also provided as a measure of performance assessment of the proposed schemes. SAC1, SAC2, ANFIS1, and ANFIS3 are intentionally suppressed in these figures for sake of clarity. It can be observed from these figures that the proposed schemes are effective in reducing both the peak displacements and accelerations under both LA10 and NF01 ground motions.

(a)

(b)

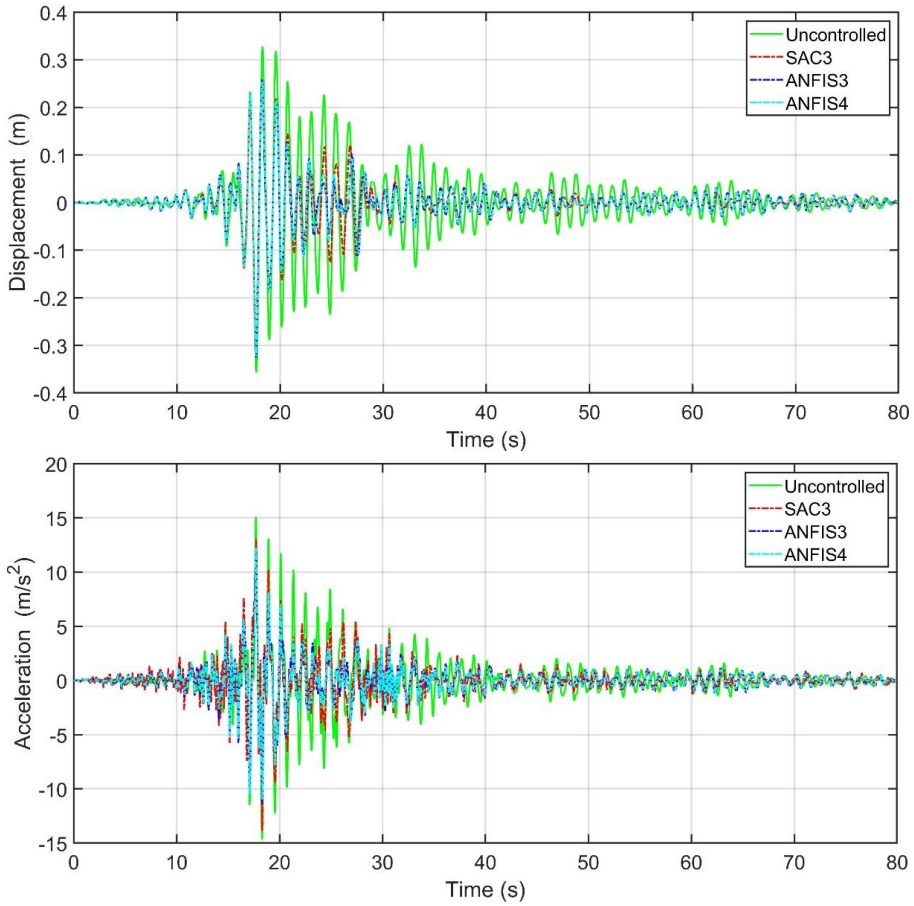

Fig. 6. Structural responses time histories of undamaged Building 1 under LA10: (a) displacement and (b) acceleration.

(a)

(b)

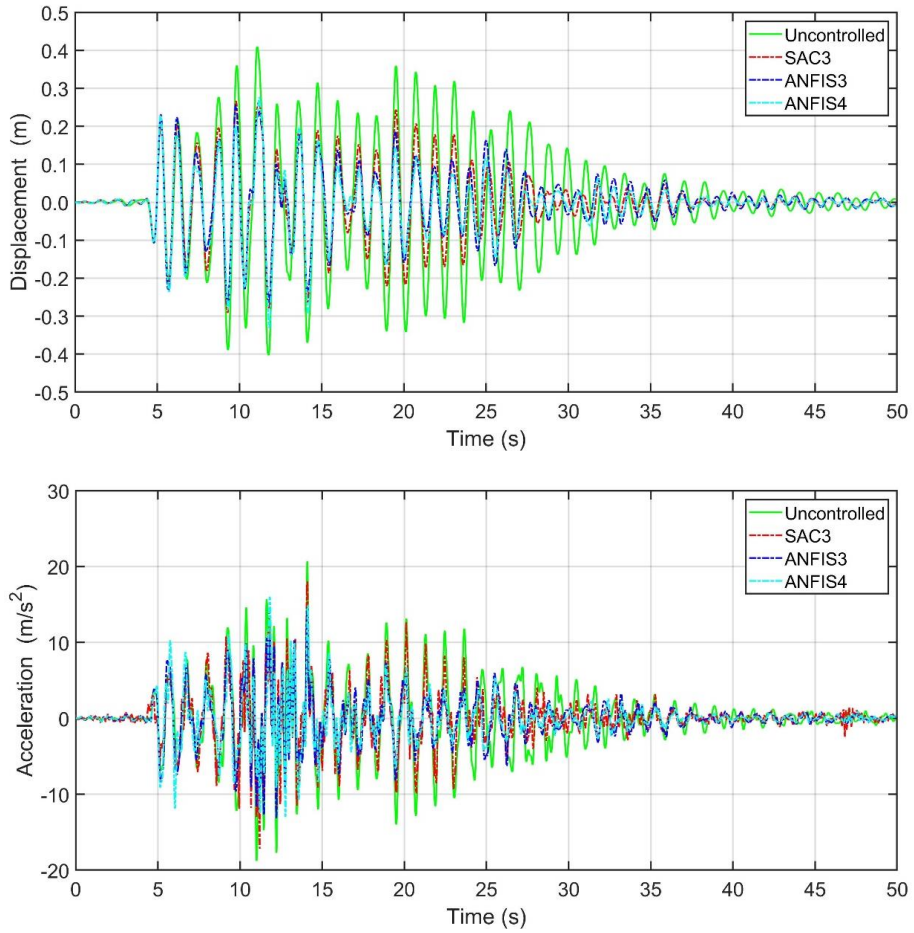

Fig. 7. Structural responses time histories of undamaged Building 1 under NF01: (a) displacement and (b) acceleration.

Fig. 8 shows the performance metrics of Building 1 for each control scheme under the seismic events. It can be observed that the performance is different from scheme to the other. For instance, the performance of SAC2 and SAC3 with respect to displacements, J_1, is different based on the feedback type. While SAC performs surprisingly good in reducing J_1 with acceleration feedback, SAC3, under all earthquakes, it exacerbates the peak displacements with displacement feedback, SAC1, under LA16 and with velocity feedback, SAC2, under and LA16 and LA23. SAC3 also surpasses all ANFIS schemes in reducing J_1.

Regarding the absolute acceleration, SAC1 worsen the index J_2 under LA23 and LS19F while SAC2 increases J_2 under all the ground motions except NF01. SAC3, on the other hand, performs much better and sustain the performance under all excitations. ANFIS1 and ANFIS3 reduce J_2 quite well in all cases except under LA23 where there is a small increase in the peak acceleration. Other ANFIS schemes did poorly under some earthquakes. SAC2 and ANFIS4 produce one data point greater than unity associated with peak drift and peak base shear, respectively under LA23. SAC1 performs poorly under many earthquakes in reducing J_3 and J_4. The rest of data points for all schemes are less than unity meaning that there is a reduction in the peak values of inter-story drift and base shear, respectively. It can be observed that SAC3 is the

only scheme that never exacerbated the peak responses for the undamaged structure while the other schemes sometimes perform better than SAC3 and other times much worse.

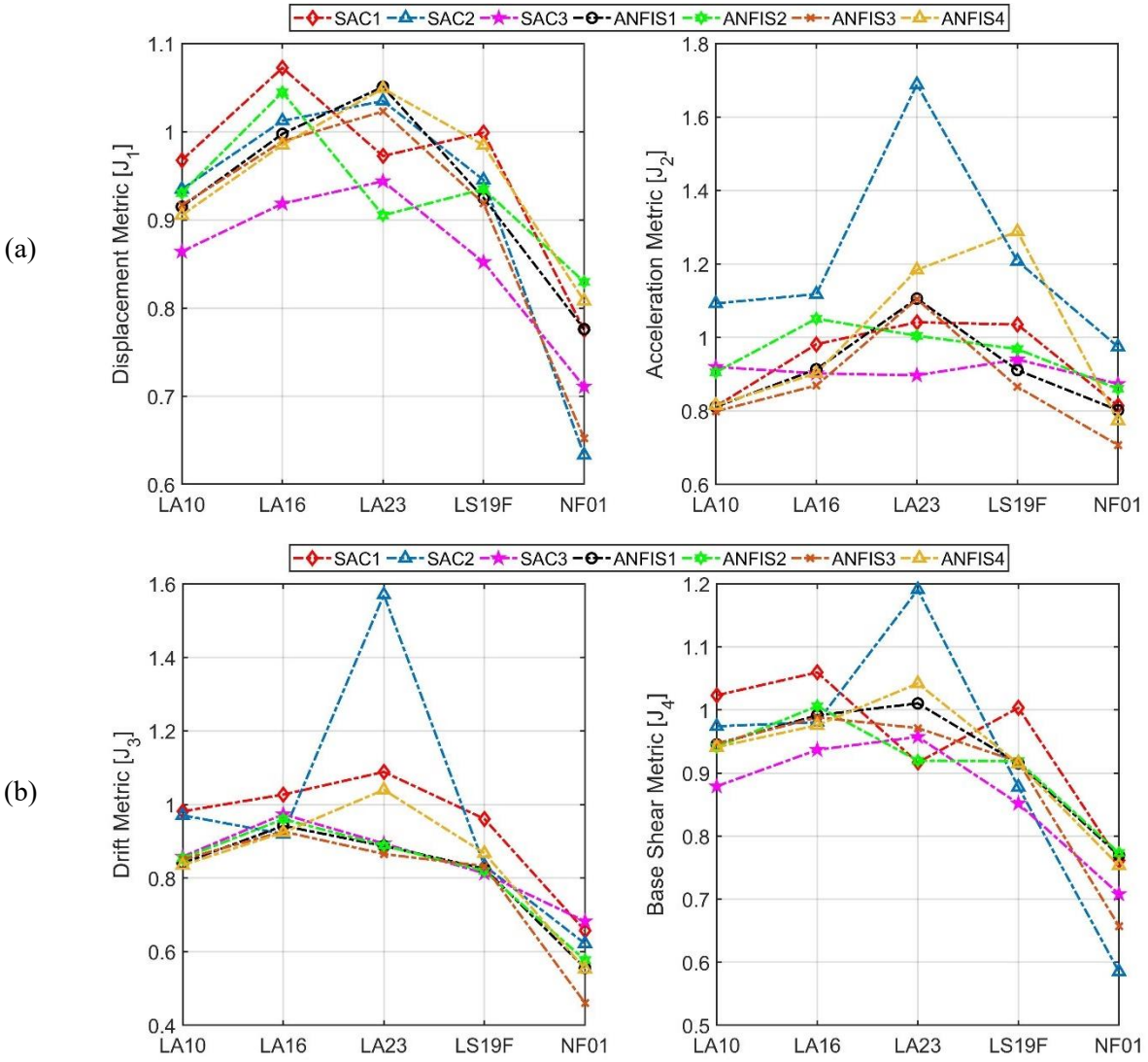

Fig. 8. Building 1 performance indices without parameter changes.

Fig. 9 displays the performance indices of Building 1 for the case associated with parameters changing. SAC with displacement feedback, SAC1, surpasses all other schemes in reducing J_1, J_2, and J_3. Moreover, the other control cases reflect an enhancement in the displacement criteria, J_1, except SAC2 under LA23 where there is an increase in the peak displacement. ANFIS schemes perform better than SAC2 and SAC3 in reducing the peak displacement for the damaged structure. For the absolute acceleration index, J_2, SAC2, and ANFIS4 perform poorly under some earthquakes while they enhance the performance under other excitations. In reducing the peak acceleration, ANFIS1 and ANFIS2 seem to surpass all other schemes for this case. For the inter-story drift index, J_3, SAC2 is the only scheme that has one data point off the threshold under LA23 earthquake regarding J_3 and J_4, respectively while all other schemes perform quite well in minimizing these indices.

(a)

(b)

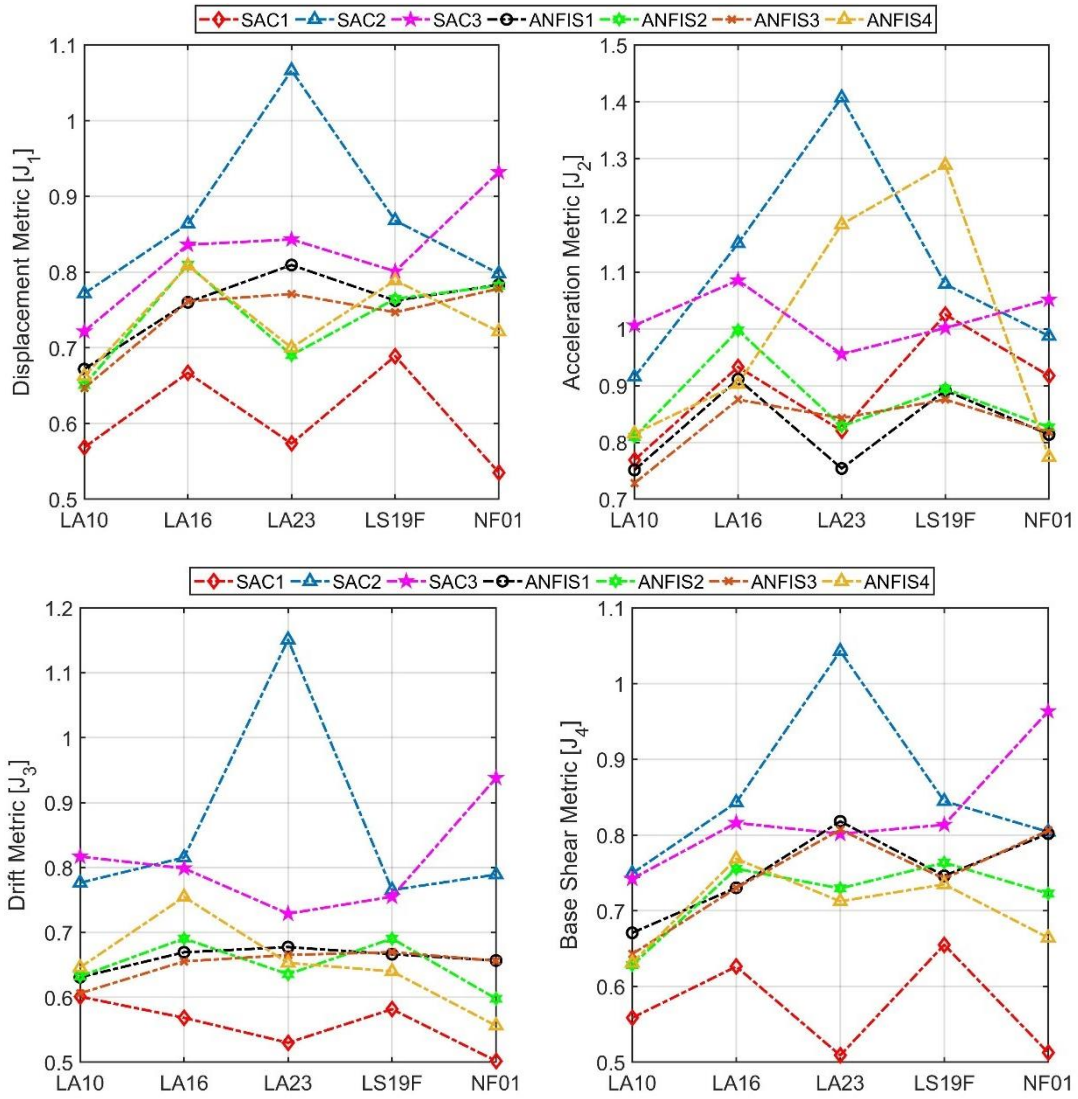

Fig. 9. Building 1 performance indices in the presence of parametric changing.

In order to further evaluate the performance of the proposed adaptive control methods, RMS of the top floors' displacements of Building 1 and 2 is calculated and depicted in Fig. 10 and Fig. 11, respectively. Fig. 10 shows RMS responses for the undamaged structure. In this figure, the results indicate that all the proposed control schemes are successful in reducing the overall responses under all earthquakes considered in the current study. ANFIS4 performs better than the other schemes in reducing the overall responses of both buildings and sustaining the performance under all earthquakes. SAC2 competes well with ANFIS4, except under LA10, in Building 1, but the latter scheme significantly outweighs the scale in Building 2. SAC1 does not perform that good compared with the other schemes. The performance of the other schemes is not the same from one building to the other. Fluctuation of the control schemes performances between Building 1 and 2 comes from the fact that the dynamics of each building is highly impacted by the motion of the other building.

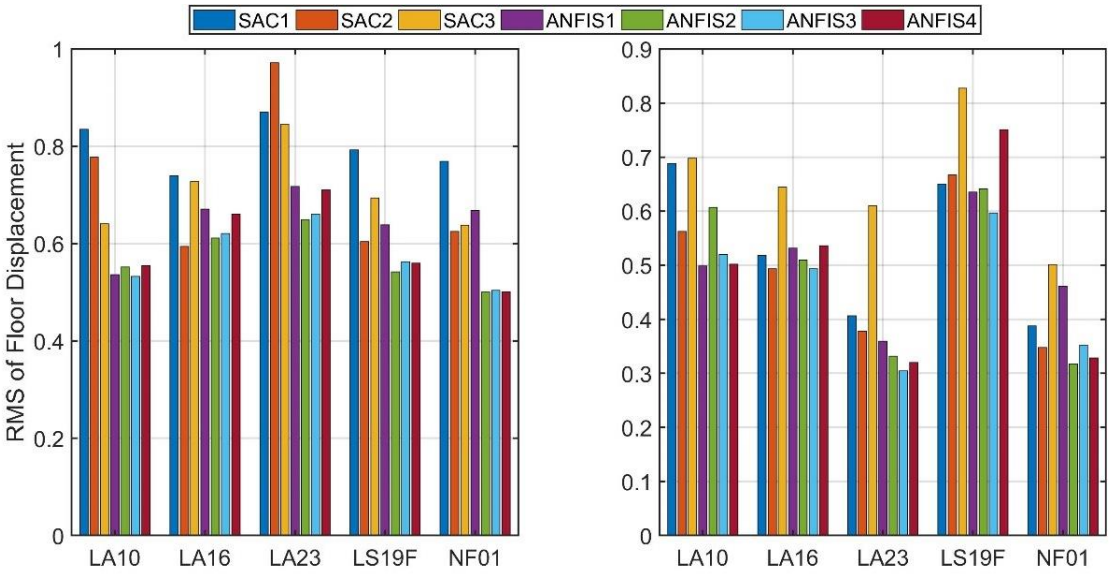

Fig. 10. RMS of the undamaged top floors displacements: (a) Building 1 and (b) Building 2.

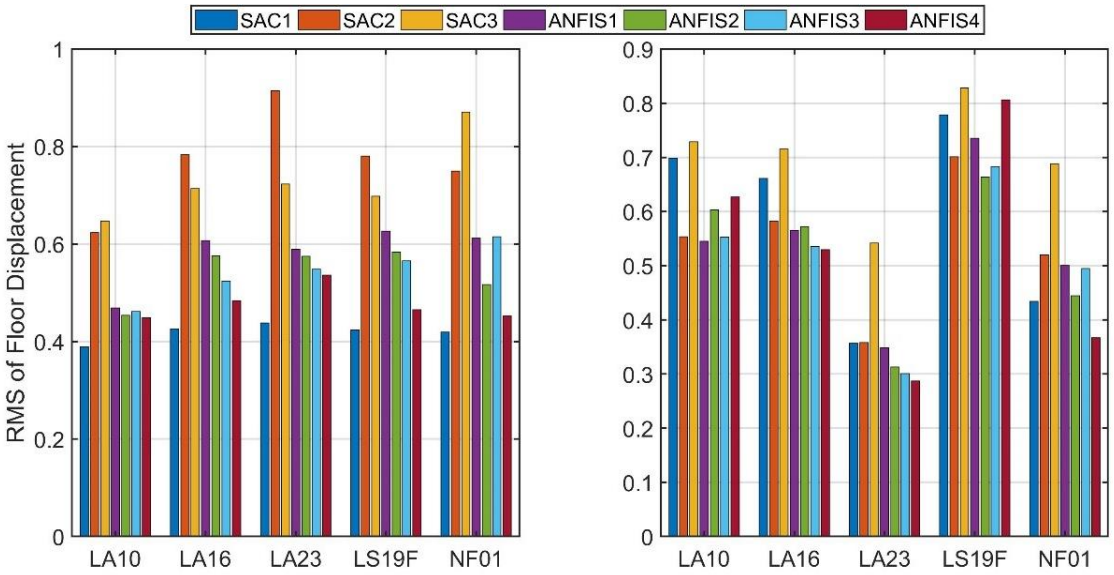

Fig. 11. RMS of the damaged top floors displacements: (a) Building 1 and (b) Building 2.

Table 3
Average reductions of all schemes for Building 1 (undamaged).

Scheme	J_1	J_2	J_3	J_4	RMS-B_1	RMS-B_2
SAC1	0.957	0.937	0.943	0.953	0.801	0.530
SAC2	0.912	1.217	0.984	0.922	0.715	0.490
SAC3	0.858	0.907	0.844	0.867	0.709	0.656
ANFIS1	0.933	0.909	0.810	0.927	0.646	0.497
ANFIS2	0.929	0.958	0.820	0.912	0.571	0.481
ANFIS3	0.900	0.869	0.787	0.896	0.576	0.453
ANFIS4	0.947	0.993	0.844	0.925	0.597	0.487

Table 4
Average reductions of all schemes for Building 1 (damaged).

Scheme	J_1	J_2	J_3	J_4	RMS-B_1	RMS-B_2
SAC1	0.607	0.893	0.557	0.572	0.419	0.586
SAC2	0.874	1.108	0.860	0.857	0.770	0.543
SAC3	0.827	1.020	0.808	0.827	0.731	0.701
ANFIS1	0.757	0.825	0.660	0.754	0.581	0.539
ANFIS2	0.740	0.871	0.649	0.720	0.541	0.519
ANFIS3	0.741	0.828	0.651	0.746	0.543	0.513
ANFIS4	0.736	0.982	0.650	0.702	0.477	0.523

Table 5
Performance metrics for Building 2 (parentheses represent the damaged structure).

Earthquake	Scheme	J_1	J_2	J_3	J_4
LA10	SAC1	0.923 (0.947)	1.205 (1.077)	1.036 (0.977)	0.927 (1.034)
	SAC2	0.815 (0.840)	1.391 (1.094)	1.118 (0.842)	0.825 (0.837)
	SAC3	1.207 (0.915)	1.690 (1.190)	1.356 (0.983)	1.209 (0.975)
	ANFIS1	0.943 (0.893)	1.127 (0.868)	1.134 (0.887)	0.956 (0.923)
	ANFIS2	1.313 (1.100)	1.368 (1.053)	1.349 (1.069)	1.317 (1.099)
	ANFIS3	0.998 (0.893)	1.147 (0.862)	1.155 (0.880)	0.996 (0.912)
	ANFIS4	0.882 (1.105)	1.034 (1.005)	1.049 (1.023)	0.897 (1.154)
LA16	SAC1	0.779 (0.849)	0.786 (0.789)	0.674 (0.659)	0.823 (0.898)
	SAC2	0.836 (0.782)	0.845 (0.740)	0.702 (0.717)	0.877 (0.825)
	SAC3	0.947 (0.842)	0.978 (0.909)	0.782 (0.936)	0.998 (0.888)
	ANFIS1	0.860 (0.766)	0.669 (0.597)	0.695 (0.620)	0.904 (0.809)
	ANFIS2	0.833 (0.731)	0.704 (0.556)	0.734 (0.581)	0.878 (0.783)
	ANFIS3	0.860 (0.766)	0.655 (0.581)	0.659 (0.587)	0.911 (0.809)
	ANFIS4	0.843 (0.720)	0.669 (0.825)	0.664 (0.585)	0.890 (0.770)
LA23	SAC1	0.501 (0.528)	0.509 (0.493)	0.520 (0.481)	0.498 (0.542)
	SAC2	0.533 (0.499)	0.554 (0.527)	0.584 (0.457)	0.522 (0.507)
	SAC3	0.735 (0.727)	0.750 (0.779)	0.765 (0.775)	0.729 (0.717)
	ANFIS1	0.513 (0.517)	0.508 (0.530)	0.503 (0.524)	0.515 (0.515)
	ANFIS2	0.553 (0.511)	0.553 (0.445)	0.555 (0.448)	0.557 (0.525)
	ANFIS3	0.479 (0.450)	0.493 (0.503)	0.486 (0.500)	0.476 (0.440)
	ANFIS4	0.552 (0.441)	0.661 (0.485)	0.673 (0.479)	0.556 (0.434)
LS19F	SAC1	0.981 (1.012)	1.102 (1.053)	1.039 (1.034)	0.972 (1.005)
	SAC2	1.067 (1.004)	1.193 (1.088)	1.101 (1.017)	1.071 (1.000)
	SAC3	1.194 (1.066)	1.288 (1.164)	1.160 (1.094)	1.198 (1.060)
	ANFIS1	1.099 (1.005)	1.086 (1.002)	1.101 (1.012)	1.096 (1.002)
	ANFIS2	1.137 (0.974)	1.168 (1.003)	1.183 (1.015)	1.128 (0.964)
	ANFIS3	1.072 (0.968)	1.014 (0.959)	1.036 (0.969)	1.079 (0.966)
	ANFIS4	1.155 (1.038)	1.189 (1.142)	1.200 (1.131)	1.145 (1.020)
NF01	SAC1	0.554 (0.482)	0.829 (0.632)	0.658 (0.464)	0.524 (0.500)
	SAC2	0.429 (0.539)	0.713 (0.653)	0.539 (0.594)	0.411 (0.533)
	SAC3	0.623 (0.719)	0.902 (0.888)	0.733 (0.723)	0.604 (0.727)
	ANFIS1	0.600 (0.563)	0.690 (0.597)	0.691 (0.580)	0.585 (0.567)
	ANFIS2	0.439 (0.504)	0.523 (0.527)	0.524 (0.529)	0.429 (0.505)
	ANFIS3	0.515 (0.548)	0.634 (0.624)	0.633 (0.609)	0.494 (0.553)
	ANFIS4	0.478 (0.409)	0.510 (0.423)	0.499 (0.427)	0.464 (0.432)

Fig. 11 shows RMS responses for the damaged structure. Again, this figure shows that all the proposed control schemes are capable to attenuate the overall responses of both buildings under all earthquakes. However, SAC1 surpasses the other schemes in mitigating RMS displacements of Building 1 while ANFIS2 performs better for Building 2.

To evaluate all the schemes considered in the current study, the mean value of each scheme under all excitations is computed and listed in Table 3 and Table 4, respectively. For the undamaged structure, Table 3, the results of all control cases reveal a significant reduction in the seismic responses. For example, the maximum reduction of floor displacement of Building 1 is achieved by SAC3 with 85.8% overall reduction. However, ANFIS3 achieves maximum overall reduction with 86.9%. on the other hand, for the damaged structure, Table 4, maximum reduction in J_1 is achieved by SAC1 with 60.7% while ANFIS1 performs better in minimizing J_2 with 82.5% reduction.

The evaluation criteria for the undamaged and damaged Building 2 under all earthquakes are listed in Table 5. The values in the parentheses represent the results of the damaged structure.

8. Conclusions

The objective of the current study is to investigate the efficacy of two adaptive control methods that were utilized to drive MR dampers connecting two closely-spaced buildings subjected to seismic excitations. The first controller is the adaptive neuro-fuzzy control method which is used to determine the command voltage of the MR damper according to the intensity of ground motion. The adaptive neuro-fuzzy controller exploits the capability of the artificial neural networks to adjust the parameters of the fuzzy logic controller in order to reduce the error between the measured and training data. The second controller is the simple adaptive controller which produces optimum control forces to make a structure tracks the behavior of a well-designed reference-model. The aim from the developed adaptive control schemes was to alleviate the peak seismic responses as well as the overall responses of the coupled structure. The numerical simulations with several ground motions show that driving MR dampers connecting two adjacent buildings by the adaptive controllers developed in this study can effectively alleviate the seismic responses of the complex system. However, the structural performance is not the same in Building 1 and Building 2 and/or under all ground motions. Also, the results show that the type of feedback significantly impacts the performance of both adaptive methods considered in the current study.

References

[1] Barroso LR, Breneman SE, Smith HA. Evaluating the effectiveness of structural control within the context of performance-based engineering. Proc. Sixth US Natl. Conf. Earthq. Eng. Seattle, Washington, Earthq. Eng. Res. Inst., 1998.

[2] Westermo BD. The dynamics of interstructural connection to prevent pounding. Earthq Eng Struct Dyn 1989;18:687–99. doi:10.1002/eqe.4290180508.

[3] Richardson A, Walsh KK, Abdullah MM. Closed-form equations for coupling linear structures using stiffness and damping elements. Struct Control Heal Monit 2013;20:259–81.

doi:10.1002/stc.490.

[4] Seto K. Active vibration control of multiple buildings connected with active control bridges in response to large earthquakes. Proc. 1999 Am. Control Conf. (Cat. No. 99CH36251), IEEE; 1999, p. 1007–11 vol.2. doi:10.1109/ACC.1999.783192.

[5] Matsumoto Y, Fukuda Y, Doi F, Seto K. Bending and Torsional Vibration Control for Flexible Structures arranged in Parallel. Trans Japan Soc Mech Eng Ser C 1998;64:414–20.

[6] Mitsuta S, Okawa E, Seto K, Ito H. Active Vibration Control of Structures Arranged in Parallel. JSME Int Journal Ser C, Dyn Control Robot Des Manuf 1994;37:436–43. doi:10.1299/jsmec1993.37.436.

[7] Yamada Y, Ikawa N, Yokoyama H, Tachibana E. Active control of structures using the joining member with negative stiffness. Proc. First World Conf. Struct. Control, vol. 2, 1994.

[8] Schurter KC, Roschke PN. Neuro-fuzzy control of structures using acceleration feedback. Smart Mater Struct 2001;10:770–9. doi:10.1088/0964-1726/10/4/322.

[9] Dyke SJ, Spencer BF, Sain MK, Carlson JD. An experimental study of MR dampers for seismic protection. Smart Mater Struct 1998;7:693–703. doi:10.1088/0964-1726/7/5/012.

[10] Abdeddaim M, Ounis A, Shrimali MK, Datta TK. Retrofitting of a weaker building by coupling it to an adjacent stronger building using MR dampers. Struct Eng Mech 2017;62:197–208. doi:10.12989/sem.2017.62.2.197.

[11] Amini F, Doroudi R. Control of a building complex with Magneto-Rheological Dampers and Tuned Mass Damper. Struct Eng Mech 2010;36:181–95. doi:10.12989/sem.2010.36.2.181.

[12] Bharti SD, Dumne SM, Shrimali MK. Seismic response analysis of adjacent buildings connected with MR dampers. Eng Struct 2010;32:2122–33. doi:10.1016/j.engstruct.2010.03.015.

[13] Bhaskararao A V, Jangid RS. Seismic response of adjacent buildings connected with dampers. 13th World Conf. Earthq. Eng., vol. 3143, 2004.

[14] Uz ME, Hadi MNS. Optimal design of semi active control for adjacent buildings connected by MR damper based on integrated fuzzy logic and multi-objective genetic algorithm. Eng Struct 2014;69:135–48. doi:10.1016/j.engstruct.2014.03.006.

[15] Gong X, Ruan X, Xuan S, Yan Q, Deng H. Magnetorheological Damper Working in Squeeze Mode. Adv Mech Eng 2014;6:410158. doi:10.1155/2014/410158.

[16] Wong CW, Ni YQ, Lau SL. Steady-State Oscillation of Hysteretic Differential Model. I: Response Analysis. J Eng Mech 1994;120:2271–98. doi:10.1061/(ASCE)0733-9399(1994)120:11(2271).

[17] Spencer BF, Dyke SJ, Sain MK, Carlson JD. Phenomenological Model for Magnetorheological Dampers. J Eng Mech 1997;123:230–8. doi:10.1061/(ASCE)0733-9399(1997)123:3(230).

[18] Barkana I. The beauty of simple adaptive control and new developments in nonlinear systems stability analysis, 2014, p. 89–113. doi:10.1063/1.4904568.

[19] Kaufman H, Barkana I, Sobel K. Direct adaptive control algorithms: theory and applications. Springer Science & Business Media; 2012.

[20] Symans MD, Kelly SW. Fuzzy logic control of bridge structures using intelligent semi-active seismic isolation systems. Earthq Eng Struct Dyn 1999;28:37–60. doi:10.1002/(SICI)1096-9845(199901)28:1<37::AID-EQE803>3.0.CO;2-Z.

[21] Choi K-M, Cho S-W, Jung H-J, Lee I-W. Semi-active fuzzy control for seismic response reduction using magnetorheological dampers. Earthq Eng Struct Dyn 2004;33:723–36. doi:10.1002/eqe.372.

[22] Burns R. Advanced control engineering. Elsevier; 2001.

[23] Al-Fahdawi OAS, Barroso LR, Soares RW. Utilizing the Adaptive Control in Mitigating the Seismic Response of Adjacent Buildings Connected with MR Dampers. 2018 Annu. Am. Control Conf., IEEE; 2018, p. 912–7. doi:10.23919/ACC.2018.8431135.

[24] Soares RW, Barroso LR, Al-Fahdawi OAS. Simple Adaptive Control Strategy Applied to Reduce

Response of Bridge Structure Subjected to Changes in Plant. 2018 Annu. Am. Control Conf., IEEE; 2018, p. 86–91. doi:10.23919/ACC.2018.8431623.

[25] Ulrich S, Hayhurst DL, Saenz Otero A, Miller D, Barkana I. Simple Adaptive Control for Spacecraft Proximity Operations. AIAA Guid. Navig. Control Conf., Reston, Virginia: American Institute of Aeronautics and Astronautics; 2014. doi:10.2514/6.2014-1288.

[26] Bitaraf M, Hurlebaus S, Barroso LR. Active and Semi-active Adaptive Control for Undamaged and Damaged Building Structures Under Seismic Load. Comput Civ Infrastruct Eng 2012;27:48–64. doi:10.1111/j.1467-8667.2011.00719.x.

[27] Amini F, Bitaraf M, Eskandari Nasab MS, Javidan MM. Impacts of soil-structure interaction on the structural control of nonlinear systems using adaptive control approach. Eng Struct 2018;157:1–13. doi:10.1016/j.engstruct.2017.11.071.

[28] Al-Fahdawi OAS, Barroso LR, Soares RW. Simple adaptive control method for mitigating the seismic responses of coupled adjacent buildings considering parameter variations. Eng Struct 2019;186:369–81. doi:10.1016/j.engstruct.2019.02.025.

[29] Jang J-S. ANFIS: adaptive-network-based fuzzy inference system. IEEE Trans Syst Man Cybern 1993;23:665–85.

[30] Jang JSR, Sun CT, Mizutani E. Neuro-Fuzzy and Soft Computing-A Computational Approach to Learning and Machine Intelligence [Book Review]. IEEE Trans Automat Contr 1997;42:1482–4. doi:10.1109/TAC.1997.633847.

[31] Schurter KC, Roschke PN. Neuro-fuzzy control of structures using magnetorheological dampers. Proc. 2001 Am. Control Conf. (Cat. No.01CH37148), IEEE; 2001, p. 1097–102 vol.2. doi:10.1109/ACC.2001.945866.

[32] BAR-KANA I, GUEZ A. Simple adaptive control for a class of non-linear systems with application to robotics. Int J Control 1990;52:77–99. doi:10.1080/00207179008953525.

[33] Ioannou PA, PV K. Adaptive systems with reduced models 1983.

[34] Ramallo JC, Johnson EA, Spencer BF. “Smart” Base Isolation Systems. J Eng Mech 2002;128:1088–99. doi:10.1061/(ASCE)0733-9399(2002)128:10(1088).

[35] Spencer BF. Reliability of Randomly Excited Hysteretic Structures. vol. 21. Berlin, Heidelberg: Springer Berlin Heidelberg; 1986. doi:10.1007/978-3-642-82863-8.

[36] Tse T, Chang CC. Shear-Mode Rotary Magnetorheological Damper for Small-Scale Structural Control Experiments. J Struct Eng 2004;130:904–11. doi:10.1061/(ASCE)0733-9445(2004)130:6(904).

[37] Al-Fahdawi OAS, Barroso LR, Soares RW. Simple adaptive control for enhancing the seismic performance of nonlinear coupled buildings with smooth hysteretic behavior. Eng Struct 2019;191:536–548.